Energy 212 (2020) 118557

Contents lists available at ScienceDirect

Energy

journal homepage: www.elsevier.com/locate/energy

Optimal dispatching strategy of regional micro energy system with compressed air energy storage

Xin Ma, Chenghui Zhang*, Ke Li**, Fan Li, Haiyang Wang, Jianfei Chen

School of Control Science and Engineering, Shandong University, Jinan, 250061, PR China

ARTICLE INFO

Article history:
Received 3 March 2020
Received in revised form
15 July 2020
Accepted 2 August 2020
Available online 15 August 2020

Keywords:
Compressed air energy storage
Thermoeconomic analysis
Variable operating conditions
Optimal dispatching
Parallel computing

ABSTRACT

The regional micro energy system (RMES) can meet users' multi-energy demand and realize the accommodation of renewable energy, which makes it a very promising energy utilization scheme. This paper presents a novel RMES structure with compressed air energy storage system (CAES) as the core energy storage component. Additionally, a bi-level optimal dispatching strategy for realizing the balance between supply and demand in regional micro energy system with compressed air energy storage system is proposed for the new scheme. The upper layer optimization calculates the optimal initial value of energy state of CAES in each energy supply cycle, and the lower layer optimizes the hourly operation strategy based on the thermoeconomic characteristics. An improved thermoeconomics method was introduced to reduce the dimensionality of the optimization model and increase the computational efficiency. The addition of parallel computing methods further accelerates the model calculation speed. Case studies demonstrate the effectiveness of the method. The proposed dispatching strategy based on thermoeconomics provides theoretical support for the application of CAES in multi-energy utilization scenarios, and provides a reference for the calculation of the revenue and payback period of the RMES.

1. Introduction

In recent years, owing to the energy security and environmental concerns, accelerating the adjustment of the energy structure has become the universal consensus and objective requirement for countries around the world [1–4]. However, due to the intermittency, randomness, and volatility of renewable energy sources, their large-scale grid connections bring serious challenges to the safety of energy systems [5,6]. Therefore, regional micro energy system (RMES) with renewable energy as power generating units were developed. The schematic diagram of the RMES structure is illustrated Fig. 1. The RMES is generally located at the end of the grid, and the objects it faces can be intelligent buildings, residential communities et al. Based on the principle of cascade energy utilization, the RMES can fulfill the multi-energy demand of the users in a dynamic market environment. Its multi-energy conversion capability changes the form of renewable energy consumption from traditional power consumption to multi-energy consumption, which realizes the local production and local consumption of renewable energy, improves the efficiency of comprehensive energy utilization [7,8], and provides an important solution to the problems associated with renewable energy development.

Under the function and orientation of RMES, energy storage systems will play a more important role in meeting the requirements of energy supply in the future [9]. Correspondingly, the requirements placed on the scale, service life, economy, and safety performance of energy storage systems will also be higher. Compared with other energy storage technologies, compressed air energy storage system (CAES) has unique advantages, including the larger scale, longer service life, etc. [10]. Among them, the multi-stage adiabatic compressed air energy storage system (MACAES) is a clean physical energy storage technology based on CAES and thermal energy storage (TES) tanks with the output capabilities of multiple types of energy such as cooling, heating, and electricity [11]. In view of the characteristics of MACAES, connecting it to RMES in the form of multi-energy cogeneration can better meet the system's demand for energy storage. Although the MACAES is rarely used in small-scale systems, several researchers have studied the tri-generation of MACAES in recent years.

In terms of research on energy supply mode and control mode of MACAES in tri-generation scenario [12,13], proposed the concept of

* Corresponding author. Tel.: +86 0531-88395717.
** Corresponding author.
E-mail addresses: max_sdu@126.com (X. Ma), zchui@sdu.edu.cn, zchsdu@163.com (C. Zhang), like@sdu.edu.cn (K. Li).

https://doi.org/10.1016/j.energy.2020.118557
0360-5442/

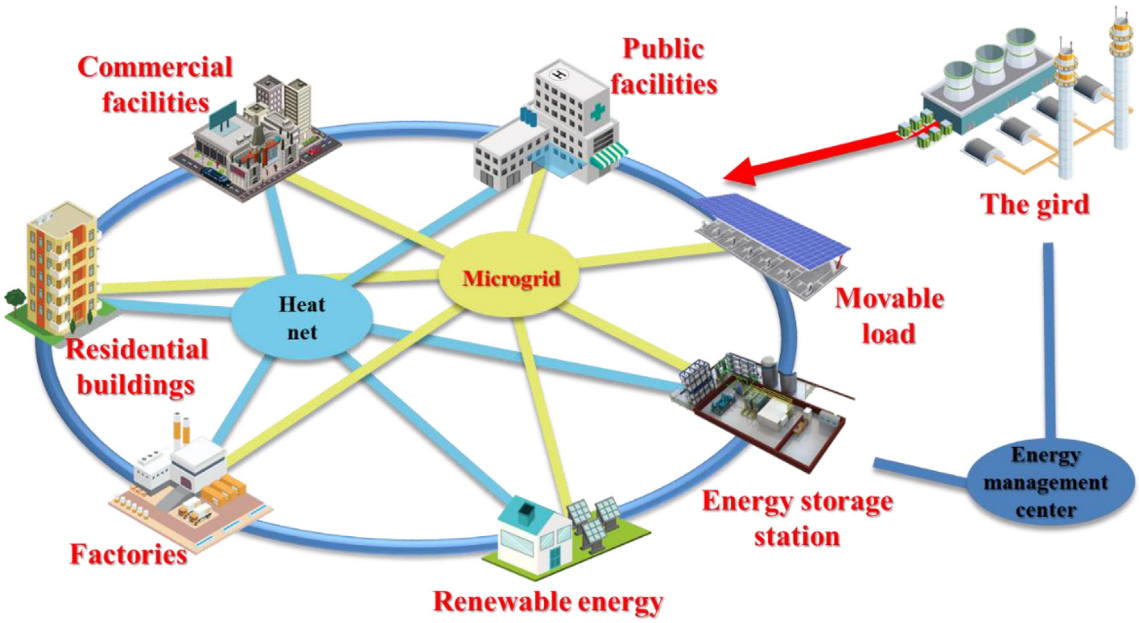

Fig. 1. Schematic diagram of regional micro energy system structure.

a trigenerative CAES compatible for a small to medium size civil application, which uses the compression heat for heating, while low-temperature exhaust air from turbine to supply cooling. Ding et al. [14–16] analyzed the comprehensive efficiency of the CAES in tri-generation operation mode and conducted an overall thermodynamic performance analysis of CAES with different structures. Lv et al. [17] proposed a CAES for tri-generation and explored the economic, social, and technological feasibility of the system through energy efficiency and economic analysis. Aiming at the CAES control problem in tri-generation scenarios, Jiang et al. [18,19] designed strategies for turbine flow control, turbine inlet pressure control, and turbine inlet temperature control to improve the performance of CAES under variable operating conditions. In terms of research on performance improvement coupling with other energy supply systems. Han et al. [20–22] conducted a case study on CAES coupled with the combined cooling and heating system (CCHP). Furthermore, a novel CCHP based on small-scale CAES is proposed in Ref. [23,24]. The sensitivity analysis was performed to compare the effects of different parameters on the thermodynamic performance of the system, and the trade-off between the thermodynamic and economic performances is investigated by an evolutionary multi-objective algorithm. Jabari et al. [25] proposed a micro energy system for the residential energy sector. Considering CAES power constraints, storage constraints, air balance constraints, etc., a mixed integer nonlinear programming was established to optimize the output of each component and reduce total energy procurement costs. Yan et al. [26] proposed a small-scale CCHP system integrated with CAES. Considering the constraints such as power constraints, energy balance of CAES gas tank et al., the multi-objective optimization model with minimizing the total cost and emissions had been set up. The improved NSGA-II optimization method is employed to obtain the system capacity and operating parameters. Wang et al. [27] proposed a CCHP system, integrated CAES and the organic Rankine cycle (ORC). Off-design model is established to study the operating characteristics of the system under all operating conditions.

Previous research laid the foundation for the application of the MACAES technology in micro energy systems. However, the concept of RMES has been introduced only recently, there are still some shortcomings in the existing research. Firstly, in terms of the performance analysis, the existing studies focus on the changes in the thermodynamic performance, but rarely involve the changes in the operating economy under variable operating conditions. In fact, as a key support for analyzing the economics of RMES, studying the variation law of economy of the MACAES energy supply is crucial for formulating RMES scheduling strategy. Besides, in the selection of optimization objectives, the available literature mostly selected maximum energy supply efficiency and optimal economy as the objectives. In the process of multi-objective optimization, the choice of subjective weight value affects the objectivity of the results to some extent. In addition, to ensure the continuity of RMES operations, the available literature introduces constraints when formulating the optimization strategies to limit the offset of MACAES's state of energy (SOE) within an operating cycle. However, according to the operating characteristics of MACAES, its energy supply efficiency will change under different SOE values, which makes the initial selection of SOE important for the economy and the efficiency of the RMES operation.

In this study, a RMES integrated with MACAES was designed. The main contributions of this study can be summarized as follows.

(1) This paper introduced the thermoeconomic evaluation method into MACAES performance analysis, and studied on the variation rules of MACAES energy supply cost and system efficiency with operating conditions
(2) The objective function constructed based on thermoeconomics cost organically combined energy efficiency indicators with economic indicators, making the optimization results more objective.
(3) A bi-level optimization management strategy was established in this paper. The upper-level obtained the optimal initial SOE value of gas tank for each energy supply cycle; the lower-level mainly considered the off-design characteristics of MACAES, and calculated the hourly output of each component.
(4) In order to speed up the calculation, an improved thermoeconomic calculation method is proposed, which saved the calculation time of MACAES energy supply cost through

simplifing the system structure. In addition, the CPU-based multithreading technology is introduced to accelerate solution.

The remainder of this paper is organized as follows. Section 2 introduces the basic framework of the proposed RMES and its operating mechanisms. Section 3 describes the mathematical model of the CAES and each of its sub-supply units. In section 4, we analyze the operating characteristics of CAES under different operating conditions based on thermoeconomics. In section 5, we propose an optimal dispatching model of the system, and introduce the solutions for accelerating the optimization models. In section 6, we solve the optimization model based on simulated cases, and draw some general conclusions based on the results. Section 7 presents the overall conclusions.

2. System structure

This section explains the design scheme of the MACAES-RMES, and the system structure is shown in Fig. 2. The system is composed of distributed power supply units (power grids, wind farms, and photovoltaic plants), refrigeration units (electric refrigerators and absorption chillers), gas boiler heating units that use natural gas as the raw material, and energy storage units (CAES and the thermal energy storage unit).

The structure diagram of MACAES is shown in Fig. 3. It consists of a compression subsystem, an expansion subsystem, a heat-exchange subsystem, and a high-pressure gas storage subsystem.

3. Modeling the components of regional micro energy system

In order to achieve the performance analysis and operation optimization of the system, it is necessary to establish the all-condition mathematical models for each main components, including the models of energy storage units (CAES and thermal energy storage units), and sub-supply units (gas heating boilers, electric refrigerators, and absorption chillers).

3.1. Model of compressed air energy storage system

In this section, a thermodynamic model for MACAES with n-stage compression and m-stage expansion is established.

3.1.1. Thermodynamic model of compression subsystem

The input electric power at time t during the compression process is

$$P_c(t) = \sum_{i=1}^{n} \frac{q_{mc}(t) R_g T_{c,i}^{air,in} \kappa}{\eta_{c,i}(t)(\kappa - 1)} \left(\pi^{\frac{\kappa-1}{\kappa}} - 1\right) \tag{1}$$

Where $q_{mc}(t)$ is the mass flow rate of air during the compression process at time t, R_g is the ideal gas constant, $T_{c,i}^{air,in}$ is the air inlet temperature of the compressor at each stage, κ is the polytropic coefficient of the compression process, $\eta_{c,i}$ is the adiabatic efficiency of the compressor, and π is the single-stage pressure ratio.

The outlet temperature of the compressor at each stage is

$$T_{c,i}^{air,out} = T_{c,i}^{air,in} (\pi)^{\frac{\kappa-1}{\kappa}} \tag{2}$$

3.1.2. Thermodynamic model of expansion subsystem

The output electric power at time t during the expansion process is

$$P_e(t) = \sum_{j=1}^{m} \frac{\eta_{e,j}(t) q_{me}(t) R_g T_{e,j}^{air,in} \gamma}{\gamma - 1} \left(1 - \mu^{\frac{1-\gamma}{\gamma}}\right) \tag{3}$$

where $q_{me}(t)$ is the mass flow rate of air during the expansion process at time t, $T_{e,j}^{air,in}$ is the air inlet temperature of the expander at each stage, γ is the polytropic coefficient of the expansion process, $\eta_{e,j}$ is the adiabatic efficiency of the expander, and μ is the expansion ratio of each stage.

The outlet temperature of the expander at each stage is

$$T_{e,j}^{air,out} = T_{e,j}^{air,in} (\mu)^{\frac{1-\gamma}{\gamma}} \tag{4}$$

3.1.3. Thermodynamic model of heat-exchange subsystem

The model of the heat exchanger is expressed as follows [28,33]:

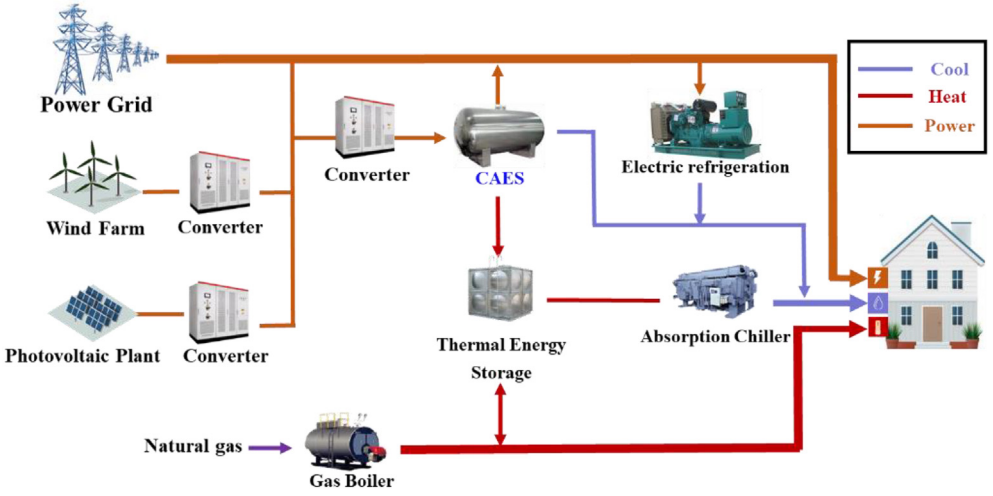

Fig. 2. Design framework of MACAES-RMES structure.

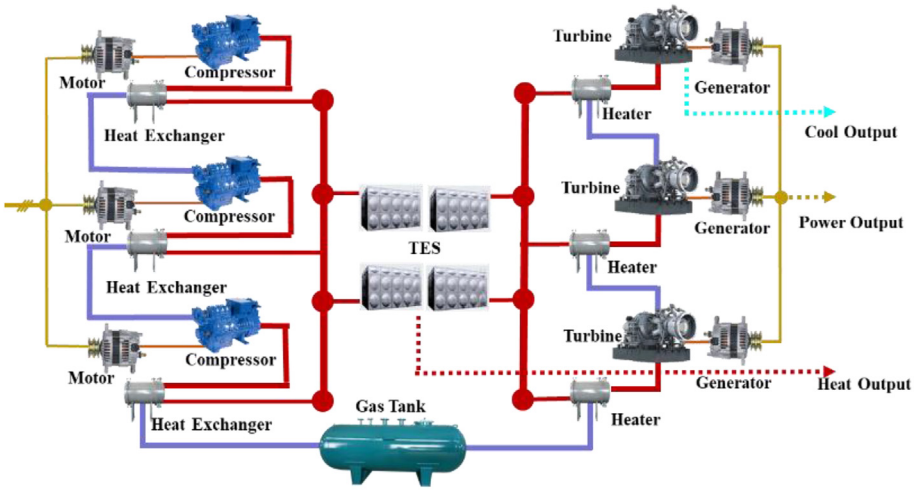

Fig. 3. MACAES structure diagram.

$$\frac{c_1 q_{m,1}(T_{1,in}-T_{1,out})}{(cq)_{\min}(T_{1,in}-T_{2,in})}=\frac{c_2 q_{m,2}(T_{2,out}-T_{2,in})}{(cq)_{\min}(T_{1,in}-T_{2,in})}=\varepsilon \tag{5}$$

$$\varepsilon=\frac{1-\exp[-NTU(1-\chi)]}{1-\chi\exp[-NTU(1-\chi)]} \tag{6}$$

$$NTU=\frac{UA}{c_{\min}} \tag{7}$$

$$\chi=\frac{c_{\min}}{c_{\max}} \tag{8}$$

where subscript 1 represents the hot fluid in the heat exchanger, 2 represents the cold fluid in the heat exchanger, c is the specific heat capacity of each fluid, q_m is the mass flow rate of each fluid, ε represents the heat-exchange efficiency of the heat exchanger, χ refers to the ratio of minimum heat capacity rate to the maximum, NTU refers to numbers of transfer unit, U is heat transfer coefficient, A refers to the heat exchange area. T_{in} and T_{out} are the inflow and outflow temperature of the fluids, respectively, and $(cq)_{\min}$ represents the minimum of the heat value between the hot and cold fluids.

The compression heat storage power of CAES at time t is

$$P_{hc}(t)=\sum_{i=1}^{n}\varepsilon(cq)_{\min}(t)\left(T_{c,i}^{air,out}-T_{c,i}^{w,in}\right) \tag{9}$$

The expansion heating power of CAES at time t is

$$P_{he}(t)=\varepsilon(cq(t))_{\min}(T_{e,j}^{w,in}-T_{stor})+\sum_{j=2}^{m}\varepsilon\left(cq(t))_{\min}\left(T_{e,j}^{w,in}-T_{e,j-1}^{air,out}\right)\right) \tag{10}$$

At any given time, only one of $q_{mc}(t)$ and $q_{me}(t)$ is greater than 0, T_{stor} is the gas storage temperature of the gas tank, $T_{c,i}^{w,in}$ is the cold water heat-exchange temperature of the compression-stage heat exchanger of each stage, $T_{e,j}^{w,in}$ is the hot water heating temperature of the expansion-stage heat exchanger of each stage, and c_p is the specific heat capacity of air.

3.1.4. System cooling model

The formula for calculating the cooling capacity at the exit of the last stage turbine is:

$$P_{caes,c}(t)=\begin{cases}0 & T_{e,m}^{w,in}>T_0\\ c_p q_{me}(t)\left(T_0-T_{e,m}^{w,in}\right) & T_{e,m}^{w,in}\le T_0\end{cases} \tag{11}$$

3.1.5. High-pressure gas storage subsystem model

The high-pressure gas storage subsystem contains a high-pressure gas tank. The pressure in the gas tank represents the storage of power in CAES. In this study, SOE_g (storage of energy of the gas tank) was used to represent the storage of power in CAES:

$$SOE_g(t)=\frac{p_{stor}(t)-p_{\min}}{p_{\max}-p_{\min}} \tag{12}$$

$$p_{stor}(t)=p_{stor}(t-1)+\int_{t-1}^{t}\frac{(q_{mc}(t-1)-q_{me}(t-1))R_g T_{stor}}{V_{stor}}dt \tag{13}$$

At any given time, only one of $q_{mc}(t)$ and $q_{me}(t)$ is greater than 0. $p_{\max}$ and $p_{\min}$ are the maximum and minimum gas storage pressure of the gas tank, respectively, and V_{stor} is the volume of the high-pressure gas tank.

3.2. Model of thermal energy storage unit

Different from the independently operating CAES, when the CAES is operating in RMES, its high-temperature thermal energy storage tank needs to be coupled with other sub-supply systems and added to the dispatching operation of RMES as an independent thermal energy storage unit. The SOE_T (storage of energy of TES) was used to represent the storage of energy of the thermal energy storage unit:

$$SOE_T(t)=\frac{Q_T(t)-Q_{T,\min}}{Q_{T,\max}-Q_{T,\min}} \tag{14}$$

$$Q_T(t) = Q_T(t-1) + \int_{t-1}^{t} \left(P_{hc}(t) + P_{hg}(t) - P_{he}(t) - P_{ha}(t)\right) dt \tag{15}$$

At any given time, only one of $P_{hc}(t)$ and $P_{he}(t)$ is greater than 0. $Q_{T,\max}$ and $Q_{T,\min}$ are the maximum and minimum heat storage capacities of the thermal energy storage tank, respectively, and $P_{hg}(t)$ and $P_{ha}(t)$ are the heating power of the gas boiler and the heat consumption power of the absorption chiller at time t, respectively.

3.3. Models of sub-supply units

The sub-supply units of the system consist of a gas heating boiler, an absorption chiller, and an electric refrigerator. The model of each unit is described as follows.

The gas boiler meets the heating demand of the users by combusting natural gas. The average heating power at time Δt is

$$P_{hg}(t) = \frac{V_g q_g \eta_g}{\Delta t} \tag{16}$$

where η_g is the heating efficiency of the gas boiler, V_g is the volume of the fuel consumed, and q_g is the heating value of the natural gas.

The absorption chiller uses the heat of the thermal energy storage unit to meet the cooling demand of the users, and its cooling power at time t is expressed as follows:

$$P_{ca}(t) = P_{ha}(t)\eta_a \tag{17}$$

where η_a is the cooling efficiency of the absorption chiller.

The electric refrigerator uses the surplus power to meet the cooling the demand of the users, and its cooling power at time t is

$$P_{ce}(t) = P_{re}(t)COP \tag{18}$$

where $P_{re}(t)$ is the power consumption of the electric refrigerator at time t, and COP is its refrigeration coefficient.

4. Operating characteristic analysis of MACAES under different operating conditions

The inherent characteristics of distributed energy such as intermittency, randomness, and volatility make RMES raise requirements for the wide-range operating capability of each unit [29]. As the core equipment of the system, reasonable analysis and evaluation of the energy supply characteristics of MACAES under variable working conditions is the premise and basis for studying the optimized operation strategy of MACAES-RMES.

4.1. Energy supply price calculation based on thermoeconomics

The exergy analysis method based on the second law of thermodynamics can reasonably describe the energy grade and is often used in MACAES thermodynamic performance evaluation. However, the simple thermodynamic analysis method does not consider the non-energy costs of the system and cannot evaluate the economic performance of the system under different operating conditions. Thermoeconomic analysis methods have recently been more frequently used for performance analysis and cost calculation of complex engineering systems [30–32]. One of the key contributions of thermoeconomics is the price valuation of exergy, which makes the exergy analysis method more practical. Since actual thermal processes are mostly irreversible, thermal processes are inevitably accompanied by exergy loss, which then becomes a significant part of the product cost. Using thermoeconomic methods, the cost formation during the entire production process can be described in detail and the price of the energy supply can be obtained. The higher the year-on-year energy supply price, the smaller the output exergy under the same non-energy cost consumption, and thus the lower the exergy efficiency of the system. Similarly, the lower the year-on-year energy supply price, the higher the exergy efficiency of the system. By using the thermoeconomic calculation method, not only can the price of the energy supply be obtained, but also can the system operating efficiency be intuitively reflected.

In order to calculate the thermoeconomic price, the exergy of each energy flux of the system under different operating conditions should be obtained. The exergy values of the air and fluid can be calculated using equations (19) and (20).

$$e_g(t) = c_p(T_g(t) - T_0) - T_0\left(c_p \ln\left(\frac{T_g(t)}{T_0}\right) - R_g \ln\left(\frac{p_g(t)}{p_0}\right)\right) \tag{19}$$

$$e_l(t) = q_l c_l T_0\left(\frac{T_l(t)}{T_0} - 1 - \ln\frac{T_l(t)}{T_0}\right) \tag{20}$$

where, e_g and e_l is the exergy of gas and exergy of fluid respectively, c_p and c_l respectively represent specific heat capacity of gas and fluid, T_g and T_l respectively represent temperature of gas and fluid, p_g is pressure of gas, T_0 is ambient temperature, and p_0 is ambient pressure.

Let E be the diagonal energy matrix whose dimensionality is the number of energy flows, and its diagonal elements are the exergy values of each energy flow. Let Z be the non-energy cost vector of each component. Event matrix A is introduced to describe the coupling relationship between each exergy flux and the subsystem of MACAES. Each row of matrix A represents the equipment, and each column represents the exergy flux. The input of exergy flux j into the subsystem i is recorded as $a_{ij} = 1$; the output from the subsystem i is recorded as $a_{ij} = -1$; no input or output is recorded as $a_{ij} = 0$. The thermoeconomic calculation model is expressed as follows:

$$A \times E \times C = Z \tag{21}$$

where C is the price matrix of each exergy flux. The cooling, heating, and power supply prices can be calculated through matrix operations.

4.2. Performance analysis of MACAES under variable operating conditions

This study takes the MACAES with four-stage compression and four-stage expansion as an example to conduct thermoeconomic calculations. The detailed performance parameters of MACAES are presented in Table 1.

The detailed calculation process of the thermoeconomic price is described in Appendix A. This section presents the analysis of the changes in each energy supply price under different operating conditions. When the electricity price is 0.3 ¥/kW·h, the results are shown in Fig. 4.

It can be seen from Fig. 4 (a) and 4 (b) that the gas storage price decreases as the SOE_g increases (gas storage pressure increases), while, the heat storage price remains constant. This is because when the final output pressure of the compressor is greater than the gas storage pressure, the secondary expansion will occur at the moment when the high-pressure air enters the gas tank, resulting

Table 1
MACAES parameters and values.

Parameter name	Value
Compression stages	4
Expansion stages	4
Maximum compression pressure/bar	200
Throttling pressure/bar	81
Mass flow rate during compression/(*kg*/*s*)	1.78
Mass flow rate during expansion/(*kg*/*s*)	2.48
Polytropic coefficient during compression/expansion	1.4
Gas tank volume/m^3	336
Compressor adiabatic efficiency	0.83
Turbine adiabatic efficiency	0.85
Heat-exchange medium	320 thermal oil
Heat-exchange efficiency of heat exchanger	0.93

in over-compression loss. The higher the gas storage pressure, the lower the overpressure loss, and the lower the corresponding gas storage price. Since the MACAES compression heat-exchange process happens before the gas storage process, the heat storage price does not change with SOE_g.

On the other hand, both the gas storage price and the heat storage price increase with the reduction of compression power, and the more the compression power deviates from the rated value, the more obvious the price increases. These trends are determined by the operating characteristics of the key components such as the compressors and heat exchangers. Under off-design operating conditions, the changes in the efficiency of compressors and heat exchangers are significant. The more the deviation from the rated value, the lower the efficiency. When the operating power is lower than the rated value by 30%, the efficiency will be lower than 50% [33]. These equipment characteristics determines the operating characteristics of MACAES under different operating conditions. When conducting operations and dispatching, it is necessary to set a light-load rate according to the actual equipment conditions.

Fig. 4(c) and (d) show that the power generation price raises up as the SOE_g increases (the gas storage pressure increases). During the expansion process, in order to ensure stable pressure, in order to ensure the stability of pressure, a throttle valve is usually set at the outlet of the gas tank, and the throttling process causes a large throttling loss. The greater the pressure difference between the two sides of the throttle valve, the greater the throttling loss, resulting in an increase in energy supply costs. Since the cooling output of the system is taken from the final-stage of the turbine outlet, the change in the throttling loss also affects the price of the cooling output, which shows a similar trend to the price of electricity output.

Similar to the compression process, the lower the expansion power than the rated value, the lower the energy conversion efficiency of the key components such as the heat exchangers and turbines, the lower the exergy efficiency of the system energy output, and the higher the price of the energy supply.

Compared with other evaluation methods, thermoeconomic evaluation method has the following advantages. Firstly, the evaluation method of thermoeconomics is based on the second law of

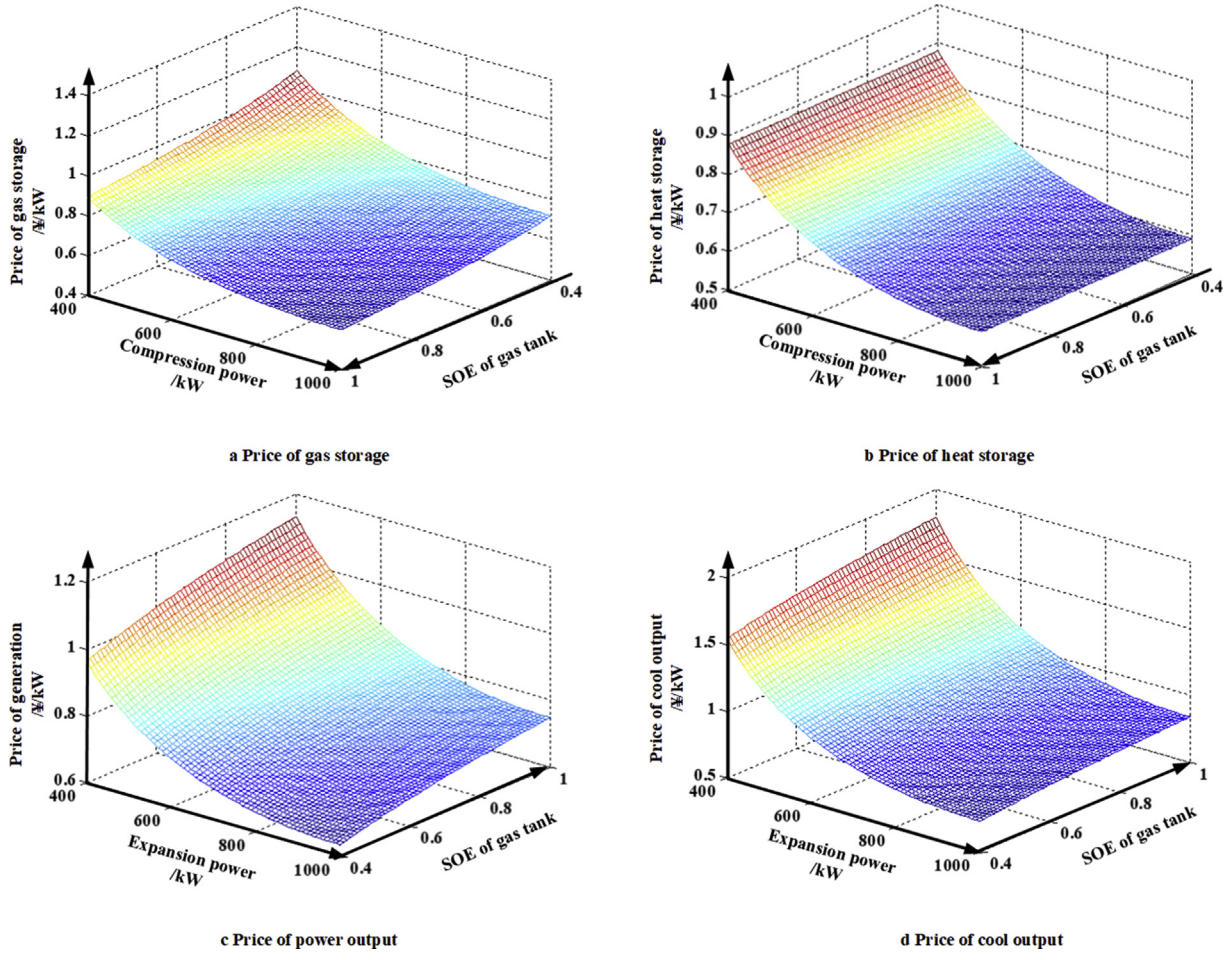

Fig. 4. Changes of energy storage and supply prices under different operating conditions.

thermodynamics, which can realize the unified quantitative description of multiple energies such as cold, heat and power. By calculating the exergy of the energy flow in real time, the thermoeconomic prices indirectly reflect the change of system efficiency through price changes, that is, the operating characteristics of the system under variable conditions. Secondly, thermoeconomics clarifies the price generation relationship between each input and output through the event matrix. Combined with the non-energy cost matrix describing the investment cost of equipment, it can describe the operating cost of the system more reasonalbe. Using this method for dispatch can more scientifically calculate the revenue and payback period of the system. In addition, taking the thermoeconomics cost as the optimization objective, the system economics and efficiency indicators can be organically combined, so that multi-objective optimization is reduced to single-objective optimization, reducing the difficulty of optimization calculation.

5. MACAES-RMES operating strategy

SOE_g of MACAES is an important parameter for RMES operation dispatching. After one operating cycle, excessive energy storage or excessive consumption will bring errors to the objective calculation of the next cycle. Therefore, when formulating the operating strategy, it is especially important to maintain the balance of the MACAES energy state during the optimization cycle. According to the thermoeconomic analysis in section 4, the change in SOE_g has a relatively large impact on the price of MACAES energy supply, and the selection of the initial SOE_g value in each energy storage cycle is key to realizing the optimal energy supply cost. Based on the system model in section 3 and the analysis results of MACAES operating characteristics under different operating conditions in section 4, in this section, a bi-level optimization model was established with the objective of a minimum thermoeconomic energy supply cost. The upper-level optimization selects the appropriate initial SOE_g value of each energy storage cycle as the optimization variable, and the lower-level optimization determines the hourly MACAES output power according to the initial value of SOE_g given by the upper level. The optimal MACAES-RMES operation strategy was obtained by solving this model. The design framework of the operating strategy is shown in Fig. 5.

5.1. Optimization variables

The upper-level optimization variables are:

$$x = SOE_g(t_0) \tag{22}$$

The lower-level optimization variables are:

$$y = [P_c \;\; P_e \;\; U_c \;\; U_e]^T \tag{23}$$

$SOE_g(t_0)$ is the storage of the energy of the gas tank at the initial moment of an energy supply cycle. P_c, P_e, U_c, and U_e are the 24-dimensional variable vectors which represent the MACAES hourly compression power, expansion power, compression flag, and expansion flag, respectively. Among them, U_c and U_e are 0−1 variables, $U_c(t)$ is 1 for compression, $U_e(t)$ is 1 for expansion, and when both of them are 0, MACAES is not involved in dispatching at time t.

5.2. Optimization objective

Both upper- and lower-level optimizations in this study establish the objective functions with the aim of a minimum RMES energy supply cost. The optimization objective mainly includes the user's electricity, heating, and cooling costs, which can be expressed as:

$$C = \min\left(\sum_{t=1}^{T} C_p(t) + \sum_{t=1}^{T} C_h(t) + \sum_{t=1}^{T} C_c(t)\right) \tag{24}$$

where T is the evaluation cycle, whose step is 1 h; C is the total energy purchase costs, $C_p(t)$ is the power purchase cost at time t, $C_h(t)$ is the heating cost at time t, and $C_c(t)$ is the cooling cost at time t. Each energy cost can be expressed as follows:

$$C_p(t) = C_{caes,\,p}(t) + C_{gird,p}(t) \tag{25}$$

$$C_{caes}(t) = c_{caes,\,p}(t) P_e(t) \tag{26}$$

$$C_{gird,p}(t) = c_{gird}(t) P_{buy}(t) \tag{27}$$

where $C_{caes,\,p}(t)$ and $C_{grid,p}(t)$ are the costs of power purchased by the user from MACAES and the large power grid at time t, respectively; $c_{caes,p}(t)$ and $c_{grid}(t)$ are the MACAES power generation price and the time-of-use electricity price from the large power grid at time t, respectively; $P_{buy}(t)$ is the amount of power purchased by the user from the power grid at time t.

$$C_h(t) = C_{tes}(t) + C_{gas}(t) \tag{28}$$

$$C_{tes}(t) = c_{tes}(t) P_{tes,\,h}(t) \tag{29}$$

$$C_{gas}(t) = c_{gas} V_g(t) \tag{30}$$

where $C_{tes}(t)$ and $C_{gas}(t)$ are the costs of heating energy purchased by the user from the thermal energy storage unit and the gas heating boiler at time t, respectively; $c_{tes}(t)$ is the energy supply price of the thermal energy storage unit at time t, and c_{gas} is the price of gas; $P_{tes,\,h}(t)$ is the amount of heat purchased by the user from the thermal energy storage unit at time t; $V_g(t)$ is the volume of gas consumed by the gas heating boiler at time t.

$$C_c(t) = C_{caes,c}(t) + C_{ca}(t) + C_{ce}(t) \tag{31}$$

$$C_{caes,c}(t) = c_{caes,c}(t) P_{caes,c}(t) \tag{32}$$

$$C_{ca}(t) = c_{tes}(t) P_{ha}(t) \tag{33}$$

$$C_{ce}(t) = c_{grid}(t) P_{re}(t) \tag{34}$$

where $C_c(t)$, $C_{ca}(t)$, and $C_{ce}(t)$ are the costs of cooling energy purchased by the user from MACAES, the absorption chiller and the electric refrigerator at time t, respectively; $c_{caes,c}(t)$ is the MACAES cooling price at time t.

5.3. Constraints

According to the system model in section 3, the optimization process should satisfy the following constraints:

(1) Electric power balance

$$P_e(t) + P_{buy}(t) + P_{WT}(t) + P_{pv}(t) = load_e(t) + P_c(t) + P_{re}(t) \tag{35}$$

where $P_{WT}(t)$, $P_{pv}(t)$, and $load_e(t)$ are the wind turbine output power, photovoltaic output power, and the power load at time t, respectively.

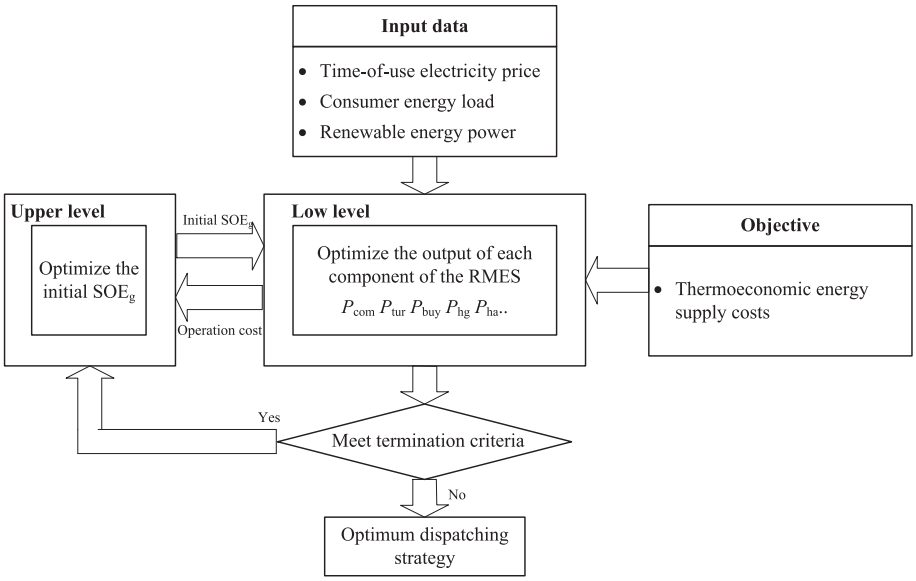

Fig. 5. Flow chart of the optimization process.

(2) Thermal balance for heating

$$P_{TES}(t) + P_{hg}(t) + P_{hc}(t) = load_h(t) + P_{he}(t) + P_{ha}(t) \tag{36}$$

where $load_h(t)$ is the heat load at time t.

(3) Thermal balance for cooling

$$P_{ce}(t) + P_{caes,c}(t) + P_{ca}(t) = load_c(t) \tag{37}$$

where $load_c(t)$ is the cooling load at time t.

(4) Power constraints of MACAES

MACAES can only be compressed or expanded at the same time. In addition, limited by the operating characteristics of key equipment such as compressors and turbines under different operating conditions, the minimum light-load power for MACAES compression and expansion needs to be set. The MACAES output constraints can be expressed as follows:

$$U_c(t)P_c^{\min} \le P_c(t) \le U_c(t)P_c^{\max} \tag{38}$$

$$U_e(t)P_e^{\min} \le P_e(t) \le U_e(t)P_e^{\max} \tag{39}$$

$$0 \le U_c(t) + U_e(t) \le 1 \tag{40}$$

(5) Gas storage unit constraints

Limited by the throttling pressure, the minimum SOE of the gas tank cannot reach 0. The SOE constraint of the high-pressure gas tank is

$$SOE_g^{\min} \le SOE_g(t) \le SOE_g^{\max} \tag{41}$$

With respect to energy storage, the offset of SOE_g is extremely important for the feasibility of scheduling [26]. To ensure the continuous operation of the RMES, the offset of SOE_g should be as small as possible within each operating cycle

$$SOE_g(t_0 + T) - SOE_g(t_0) \le \delta_{SOE} \tag{42}$$

where, T is the operation time of each cycle.

(6) Thermal energy storage unit constraint

Similar to the gas storage unit, the SOE constraint of the thermal energy storage unit is

$$0 \le SOE_{\mathrm{TES}}(t) \le SOE_{\mathrm{TES}}^{\max} \tag{43}$$

Equation (15) suggests that the heat in TES can be used for expansion heating, absorption cooling, or direct supply to the heat users. When the heat energy in the MACAES expansion process is insufficient, the turbine outlet temperature may be below 0 °C, resulting in icing or exceeded temperature resistance of the equipment. Therefore, in the heat distribution of the thermal energy storage tank, the heat required by the expansion process must be fulfilled first. When there is a competition between the heat consumption of the direct supply to the heat users and the heat consumption of absorption cooling, since the cost of cooling using electricity is lower than the cost of heating using natural gas, the heat in the TES will first fulfill the heating demand, and the remaining heat will be used for absorption cooling.

(7) Cooling unit constraints

Limited by the MACAES refrigeration capacity and the residual heat in the heat output pipe, the system uses combined electric refrigerators and absorption chillers for cooling. The output constraints of these two cooling units at each moment should be determined by the prices of their energy supply.

$$P_{ca}(t) = \begin{cases} 0 & c_{ce}(t) < c_{ca}(t) \\ load_{\mathrm{c}}(t) - P_{\mathrm{cCAES}}(t) & c_{ce}(t) > c_{ca}(t) \end{cases} \tag{44}$$

$$P_{ce}(t) = \begin{cases} load_{\mathrm{c}}(t) - P_{\mathrm{cCAES}}(t) & c_{ce}(t) < c_{ca}(t) \\ load_{\mathrm{c}}(t) - P_{\mathrm{cCAES}}(t) - P_{ca}(t) & c_{ce}(t) > c_{ca}(t) \end{cases} \tag{45}$$

5.4. Solution algorithm

In the bi-level optimization model proposed in this study, the lower-level optimization contains 0–1 integer variables and nonlinear constraints, which is a typical mixed integer nonlinear programming (MINLP). Although the model constructed by these variables is generally more complicated, its mathematical description of the actual problem is more accurate. At present, the popular algorithms for solving MINLP problems include particle swarm optimization, ant colony optimization algorithm, genetic algorithm, and gray wolf algorithm. For the initial value selection of the upper-level SOE_g, an enumeration algorithm was used in this study to conduct the optimization, and a genetic algorithm was used to solve the lower-level optimization.

For the optimization proposed in this paper, the energy balance constraint in equation (42) is a relatively strict confinement, which aggravates the degree of nonlinearity of the model and slows the solving process of the genetic algorithm. Moreover, due to the numerous system equipment and the complicated operation process of MACAES, the thermoeconomic event matrix has a high dimension, and the compute of the energy supply price is large, which further extends the optimization solution time. For upper-level optimization, each time an SOE_g initial value is given, the lower-level optimization program needs to operate once, which makes the entire optimization solution time-unacceptable.

To speed up calculations, in this paper, an improved MACAES thermoeconomics energy cost calculation method is proposed. By integrating the MACAES structure, the dimensionality of the event matrix was reduced, and the calculation time was shortened. The specific steps are as follow.

For the multi-stage structure of MACAES, with the exception of the first-stage, the working conditions (temperature, pressure ratio, and flow rate) of the subsequent stages are basically the same. Based on the above considerations, we have made the following adjustments to the system structure.

(1) Combine the subsequent compressors into a post-stage compression subsystem, and the input and output exergy of the combined system is the sum of the original each subsequent compressor.
(2) Combine the subsequent expanders into a post-stage expansion subsystem, and the input and output exergy of the combined system is the sum of the original each subsequent turbine.
(3) Combine the subsequent exchangers into a post-stage exchange subsystem, and the input and output exergy of the combined system is the sum of the original each subsequent exchanger.
(4) After the merger, the non-energy cost of each system is the sum of the original system equipment costs.

The improved MACAES structure is shown in Fig. 6 Any multi-stage structure is equivalent to a two-stage compression and two-stage expansion structure.

The improved thermoeconomic model greatly reduces the dimension of the event matrix, and the system event matrix becomes 10 × 18 dimensions. The results of the thermoeconomic calculation before and after the improvement are shown in Fig. 7 The comparison show that the calculation results of thermoeconomics are basically consistent before and after the improvement, and the rationality of the proposed improvement method is verified.

In addition, this paper introduces parallel computing into the solution process of the bi-level optimization model. Parallel computing based on the MPI interface is considered to be one of the most effective ways to speed up the optimization and solution [34].

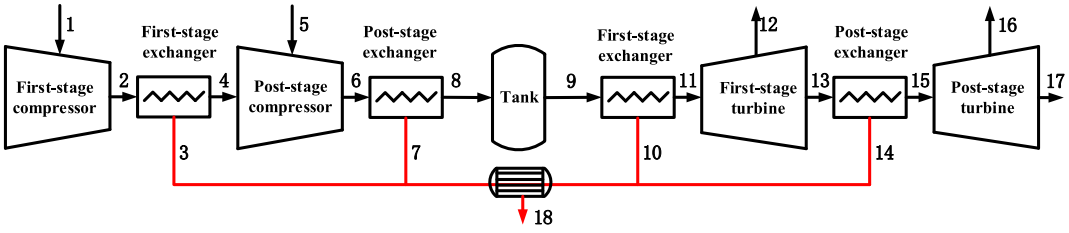

Fig. 6. Improved MACAES structure.

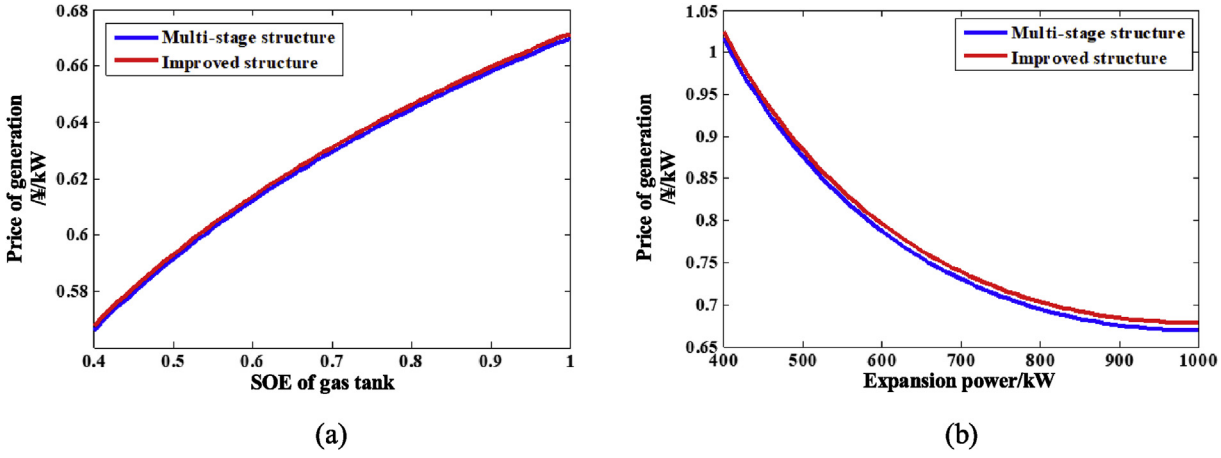

Fig. 7. Comparison of thermoeconomic calculation results.

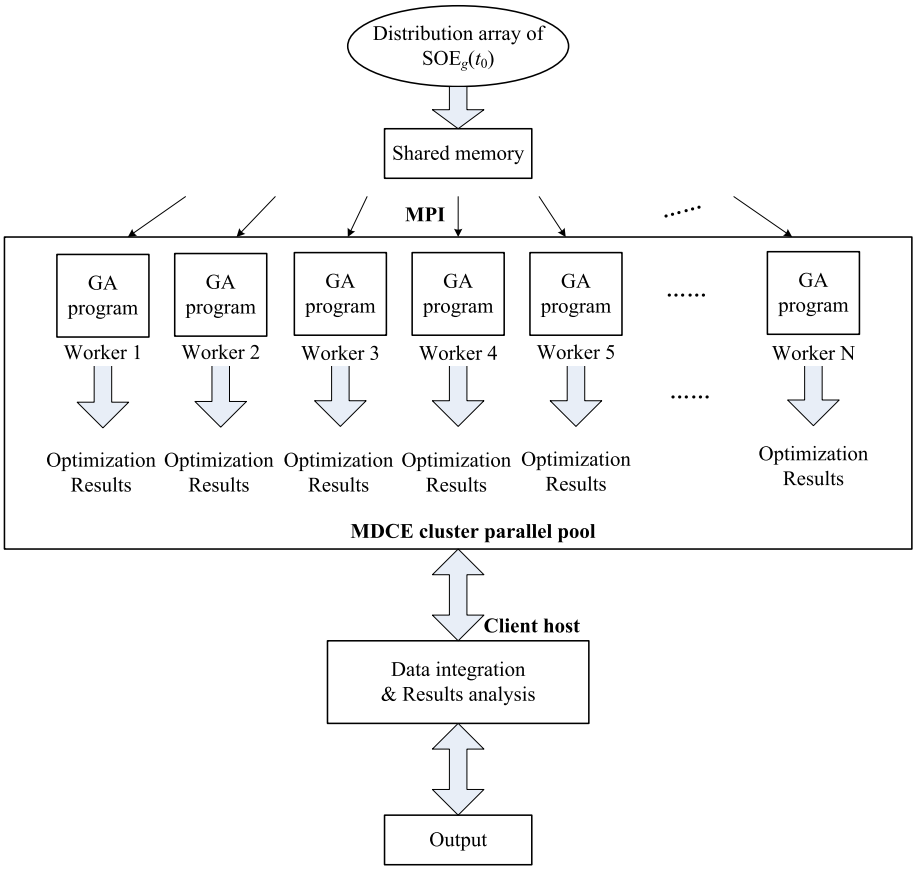

Fig. 8. Schematic diagram of parallel computing based on MPI interface.

The calculation principle is illustrated in Fig. 8.

6. Case studies

6.1. Operation conditions and system parameters

To verify the accuracy of the proposed operation strategy and the practicability of the acceleration method, using the typical summer and winter loads in southern China as an example, the MACAES-RMES structure was applied to optimize the output of each component in the system. The renewable energy power output and typical loads in summer and winter are shown in Figs. 9–12. The main design parameters of MACAES are listed in Table 1, and the initial SOE_g value of MACAES is set to the minimum value of 0.4. The operating parameters of each equipment are listed in Table 2, and the time-of-use electricity price from the power grid is shown in Fig. 13 [35–36]. The genetic algorithm has a population size of 400 and an evolutional generation of 600.

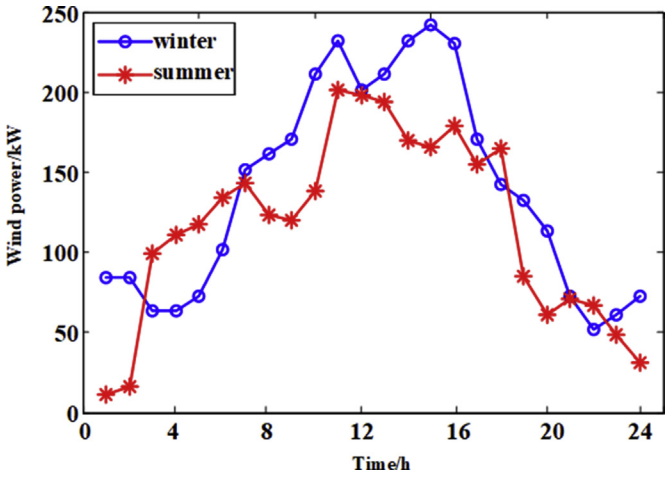

Fig. 9. Typical daily power changes of wind power generation.

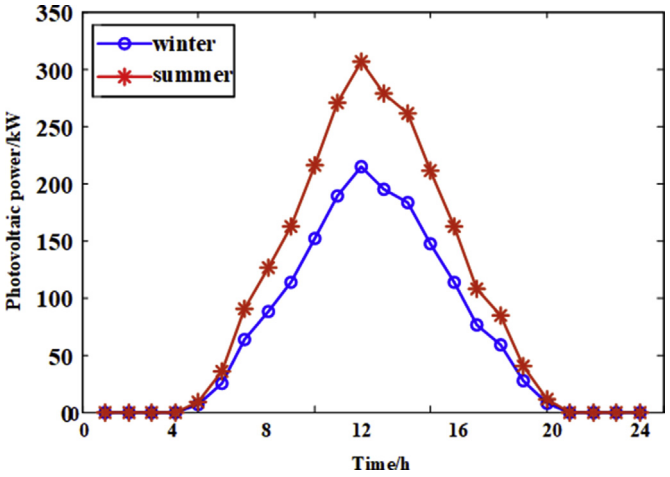

Fig. 10. Typical daily power changes of photovoltaic power generation.

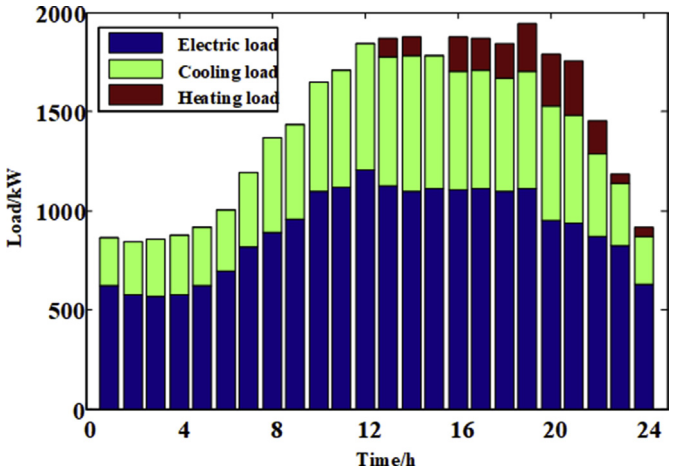

Fig. 11. Typical daily loads in summer.

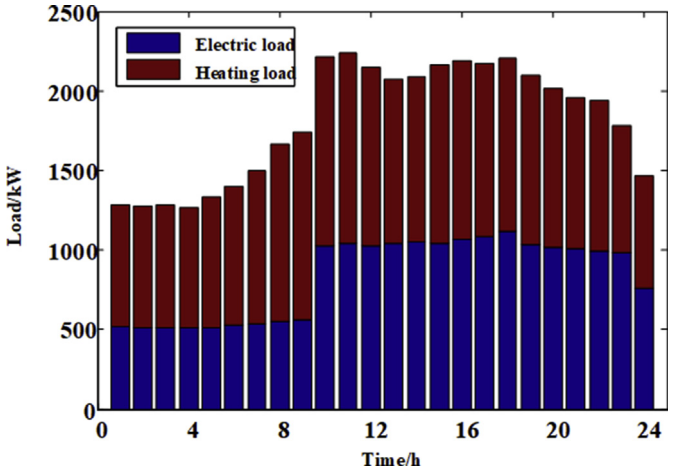

Fig. 12. Typical daily loads in winter.

6.2. Optimization results of MACAES initial storage of energy

MACAES stores energy in the low-priced periods of the electricity price and supplies power in the high-priced periods to achieve peak sheaving. The time-of-use electricity prices in Fig. 13 suggest that the daily price enters the low-priced period at 23:00. If 0:00 is selected as scheduling initial moment of each day, and the constraint that the initial value of the gas storage in each cycle is equal as stated in equation (42) is satisfied, MACAES can only compress for 1 h, which makes SOE_g change only in a thin range. In view of the above problem, in this study, the 7:00, which is the cut-off point of the first low-priced period of electricity was selected as the initial moment, and MACAES could compress for nearly 8 h from 23:00 of the previous day to 7:00 of the next day. Moreover,

Table 2
RMES equipment parameters and values.

System	Parameter	Value
Sub-supply system	Refrigeration coefficient of absorption chiller	0.9
	Refrigeration coefficient of electric refrigerator	3
	Heating efficiency of gas boiler	0.85
	Gas price (yuan/m^3)	3
MACAES	maximum energy storage power (kW)	1000
	minimum energy storage power (kW)	400
	maximum expansion power (kW)	1000
	minimum expansion power (kW)	400

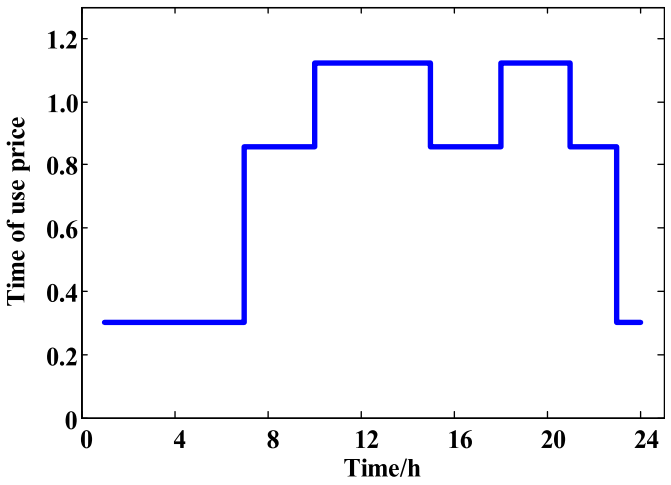

Fig. 13. Time of use electricity price.

the $SOE_g(7)$ values could be discussed in a large range. The optimization results with different $SOE_g(7)$ values under summer and winter operating conditions are shown in Fig. 14.

As shown in Fig. 14, the impact of SOE_g on the overall energy supply costs of the system is divided into multiple stages, and each stage has a trend of low and then high. The decrease in the energy supply cost of each stage is due to the higher benefits obtained by the increased energy supply duration. However, when the duration of energy supply increases to a certain level, the CAES state of energy meets the energy supply requirements for several hours, and

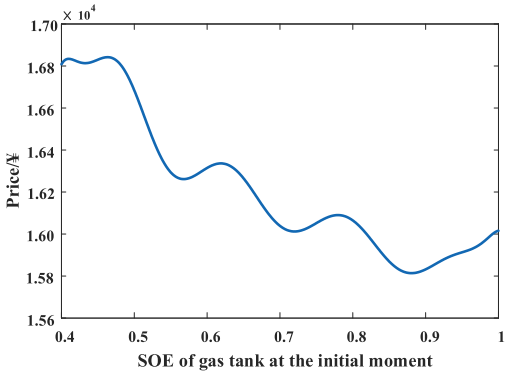

(a) Impacts of 7:00 SOE_g on optimization results under summer operating conditions

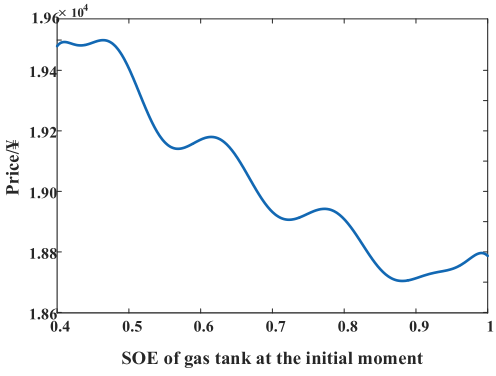

(b) Impacts of 7:00 SOE_g on optimization results under winter operating conditions

Fig. 14. Changes in optimization results with initial SOE_g values under summer and winter operating conditions.

the remaining gas volume is insufficient to reach the full load of the next hour. Then, MACAES is bound to work at low power operating conditions, the impact of increasing SOE_g on the power generation price gradually becomes apparent, and the overall costs of energy supply gradually increase. When SOE_g continues to increase, the benefits of the energy supply duration further increase, and the system energy supply costs continue to decrease. In general, the larger the initial value of SOE_g, the cheaper the energy supply costs of the system, and the greater the impact of the energy supply duration on the benefits of the system than the impact of SOE_g on the energy supply cost. For the optimal value of SOE_g at the initial moment, only the optimal value of the optimization results in the last stage, i.e., the minimum value corresponding to 0.8–1.0, should be discussed. The SOE_g value of 0.4 at 7:00 means that MACAES cannot supply energy during the high-priced period, and MACAES-RMES can only rely on the sub-supply unit to supply energy independently. The difference between the energy supply cost in this case and the optimization result under the optimal SOE_g value, that is, the operating benefit of MACAES. The minimum energy supply cost and the system benefits of RMES under summer and winter operating conditions are shown in Table 3.

6.3. Results of the optimal dispatching

Based on the given parameters and operating conditions, the output of each MACAES-RMES component in different seasons is optimized according to the dispatching model proposed in the section 5. The optimization results are presented in Figs. 15 and 16.

The optimization results of summer and winter electric power balance show that from 23:00 to 6:00, the electricity price is low, and the power of renewable energy power generation is relatively low. The system purchases electricity from the power grid to fulfill the demand of electricity users, and MACAES is compressing at the same time to store energy for the peak-period power supply. From 7:00 to 9:00, the amount of renewable energy power generation increases. The system meets the power demand of the users by wind power and photovoltaic power generation, and the power grid assists the power supply. From 10:00 to 20:00, the peak period of power consumption is entered, and the renewable energy power generation, compressed air energy storage, and the power grid operate together to supply power to electricity users. From 20:00 to 22:00, the power load is reduced, and the electricity price enters the flat-rate period. At this time, the amount of power generated by renewable energy is gradually reduced. The system purchases electricity from the power grid to fulfill the demand of electricity users, and the renewable energy power generation assists the power supply. Based on the output optimization of MACAES compression and expansion and the SOE_g value changes, the hourly changes in thermoeconomic expansion prices under typical summer and winter operating conditions are shown in Figs. 17 and 18 Among them, the power generation price before the moment of the first expansion is calculated from the SOE_g value and the rated expansion power.

Limited by the energy storage of the gas tank and the duration of power supply, MACAES cannot achieve the energy supply in all peak periods of power consumption. In order to realize maximum profitability, the energy supply periods of MACAES coincide with the two periods of high electricity price, i.e., 10:00–14:00 and 18:00–20:00. At 10:00–14:00, the outputs of wind turbines and photovoltaic systems enter the peak period, and MACAES and the power grid assist the power supply. At 18:00–20:00, the renewable energy power generation decreases sharply, the power is mainly supplied by MACAES, and the power grid and renewable energy power generation assist the power supply.

In summer, there is a large demand for the cooling load. In the periods of low electricity price, the system meets the cooling load demand with electric refrigeration, whereas in the periods of high electricity price, the system meets the cooling load demand with absorption refrigeration. The hourly price changes of electric refrigeration and absorption refrigeration are displayed in Fig. 19.

At 1:00–5:00, due to the compressed air storage feature of MACAES, the amount of heat stored in the gas tank increases, and the price decreases. The corresponding absorption refrigeration price decreases, but it is still slightly higher than the price of electric refrigeration during the flat-rate period. During the periods of 7:00–9:00, 15:00–17:00, and 21:00–22:00 with flat electricity prices, the cooling is still supplied by electric refrigeration.

Under winter operating conditions, the heat load demand is large. The capacity of the thermal energy storage tank is insufficient to fulfill the heating demand of all the users, and it is necessary to use the gas boiler for joint energy supply. At 1:00–5:00, MACAES compresses and stores heat to support the heating load.

6.4. Calculation time comparison

The computer hardware used to solve the model in this study is an 8-core Intel core I7-9700k 3.6 GHz desktop processor. Under four combinations, with or without model improvement and with or without computing acceleration, the optimization model is solved using four methods:

(1) Method 1: The traditional thermoeconomic model is used to solve the energy supply prices, and the 8-core CPU is used to solve the optimization model in a single process and a single thread serial.
(2) Method 2: The traditional thermoeconomic model is used to solve the energy supply prices, and the 8-core CPU is used to solve the optimization model in parallel.
(3) Method 3: An improved thermoeconomic model is used to solve the energy supply prices, and the 8-core CPU is used to solve the optimization model in a single process and a single thread serial.
(4) Method 4: An improved thermoeconomic model is used to solve the energy supply prices, and the 8-core CPU is used to solve the optimization model in parallel.

The calculation time of each computing method is shown in Table 4.

According to Table 4, it can be seen that the introduction of improved thermoeconomics and parallel computing has significantly reduced the calculation time. Among them, the time consumption of method 4 is only about 5% of method 1.

Table 3
Minimum energy supply costs of the system in summer and winter.

Operating conditions	Initial value of SOE_g	Energy supply cost (yuan)	Benefit (yuan)
Summer	0.881	15810	1041.1
Winter	0.881	18680	730.7

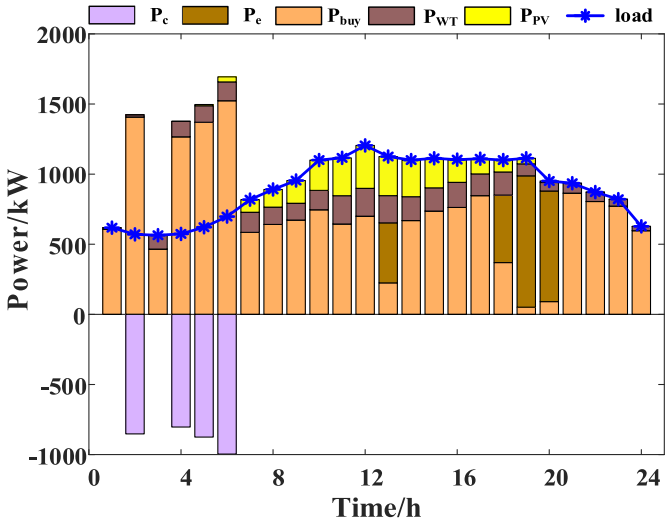

(a) Optimization results of electric power balance

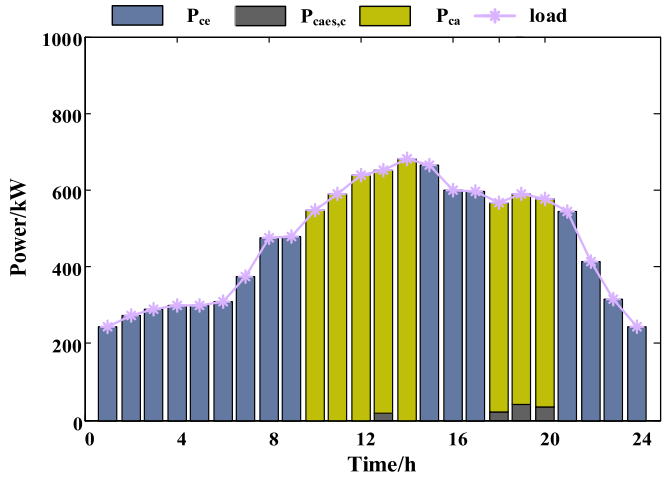

(b) Optimization results of cool balance

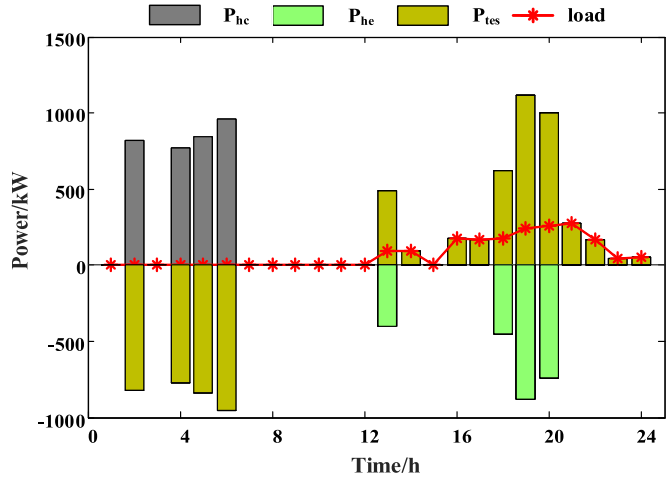

(c) Optimization results of heat balance

Fig. 15. Power, cooling, and heating optimization results under summer operating conditions.

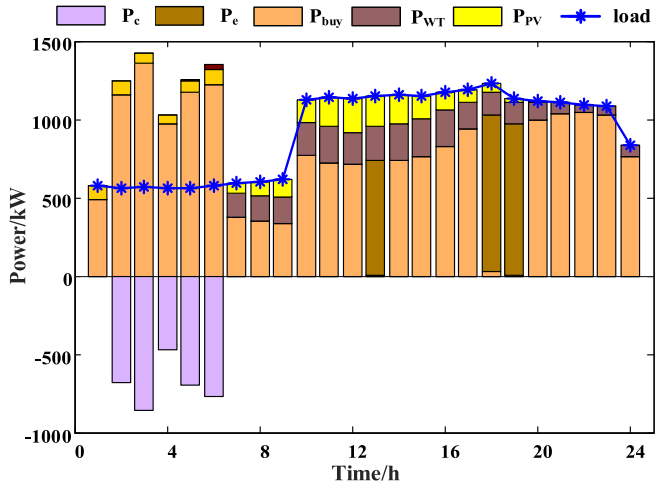

(a) Optimization results of electric balance

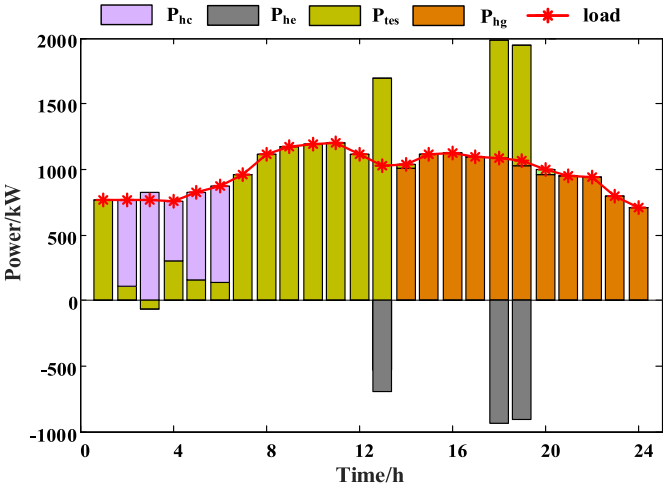

(b) Optimization results of heat balance

Fig. 16. Power and heating optimization results under winter operating conditions.

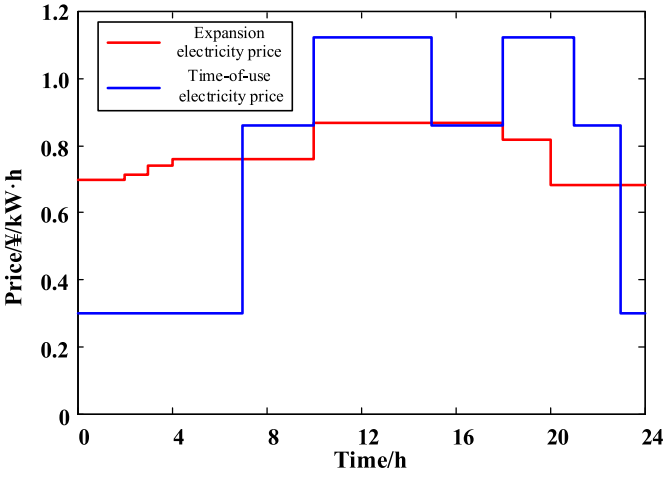

Fig. 17. Price changes of hourly expansion in summer.

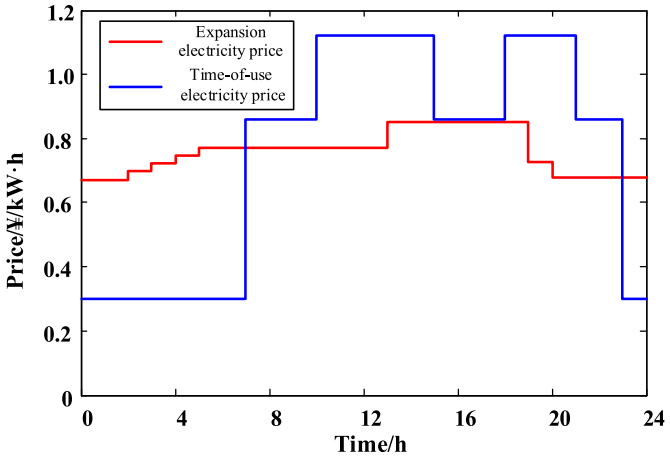

Fig. 18. Price changes of hourly expansion in winter.

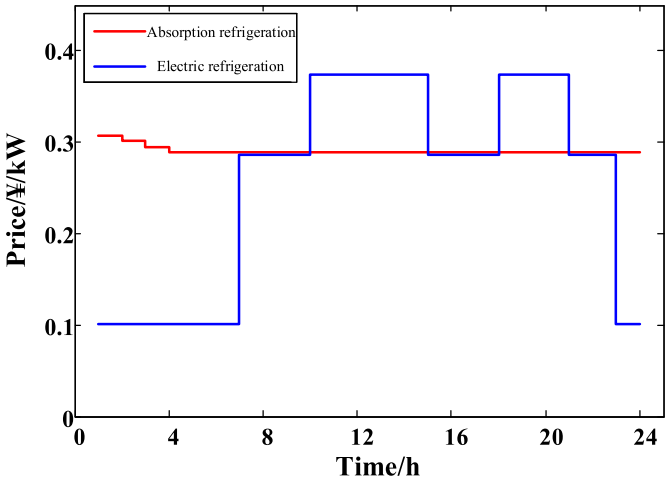

Fig. 19. Price changes of cool supply by electric refrigeration and absorption refrigeration in summer.

Table 4
Calculation time of different methods.

Operating condition	Method 1 (h)	Method 2 (h)	Method 3 (h)	Method 4 (h)
Summer	21.76	2.96	8.06	1.1
Winter	19.5	2.65	7.16	0.96

7. Conclusions

Based on the characteristics of RMES, and combined with the advantages of the large capacity of MACAES, we proposed an optimal dispatching strategy to cut off the peaks and fill in the valleys of energy supply through compressed air energy storage; increase the production, distribution, consumption, storage, and conversion of multi-energy components such as cooling, heating, and power of the system; achieve energy savings and fulfill the multi-energy demand of users. In order to discuss the operating characteristics of MACAES under different operating conditions, we analyzed the price changes in energy storage, heat storage, power generation, and refrigeration of MACAES under different values of compression and expansion power and different energy storage values of the gas tank based on the thermoeconomic evaluation method. Consequently, taking the minimum energy supply cost of the system based on thermoeconomics as the optimization objective, we established a bi-level optimization model considering the MACAES energy supply characteristics, the balance constraints of the energy storage of the gas tank in each cycle period, and the energy supply constraints of each sub-supply equipment. The optimization objective based on the thermoeconomic evaluation is organically coupled with energy supply efficiency and economy, and the two optimization objectives of the operating efficiency and system economy are combined into one, eliminating the impacts of the subjective selection of the weight values for obtaining a compromised solution as the optimization result. This makes the calculation simpler and the optimization result more objective.

Aiming at the problem that the optimization model has a large amount of data and a high degree of nonlinearity, which reduces the model solution speed, we increased the speed by improving the thermoeconomic model and adopting the CPU-based parallel computing method. Based on the typical operating conditions in summer and winter, the hourly output status of each equipment was obtained. The optimization results show that MACAES stores energy in low-priced periods, expands power generation in high-priced periods, cuts off the peaks, and fills in the valleys to achieve profitability and reduce operating costs. Based on these optimization results, according to the time-of-use electricity price and the thermoeconomic power generation price, the optimal energy storage periods and optimal power generation benefit periods of MACAES were analyzed, and the optimization analysis of the impacts of different SOE_g values at the initial moment of the gas tank on the energy supply costs of the system was conducted together with the thermoeconomic analysis, so that the optimal initial storage of energy of compressed air energy storage can be determined to realize the maximum benefits.

In this study, we applied the thermoeconomic performance calculation method to the optimal dispatching of MACAES-RMES and verified the validity of the method and the convenience of its application in optimal dispatching. The proposed dispatching strategy based on thermoeconomics and the optimization result on the initial storage of energy provide theoretical support for the application of compressed air energy storage in multi-energy utilization scenarios and provide a reference for calculating the investment costs, benefits, and payback periods of the system.

Author statement

Xin Ma: (First author) Conceptualization, Methodology, Software, Writing - original draft. Chenghui Zhang: (Corresponding author) Conceptualization, Funding acquisition, Writing- Reviewing and Editing, Li Ke: Writing- Reviewing and Editing. Fan Li: Software, Haiyang Wang: Software, Jianfei Chen: Software, Data curation

Declaration of competing interest

The authors declare that they have no known competing financial interests or personal relationships that could have appeared to influence the work reported in this paper.

Acknowledgement& Funding

This work is supported by the Foundation for Innovative Research Groups of NSFC (61821004), National Natural Science Foundation of China (61320106011, 61573223, 61733010), and fundamental research funds of Shandong University (2018JC032).

Appendix A

The workflow chart of MCAES is shown in Fig.A1.

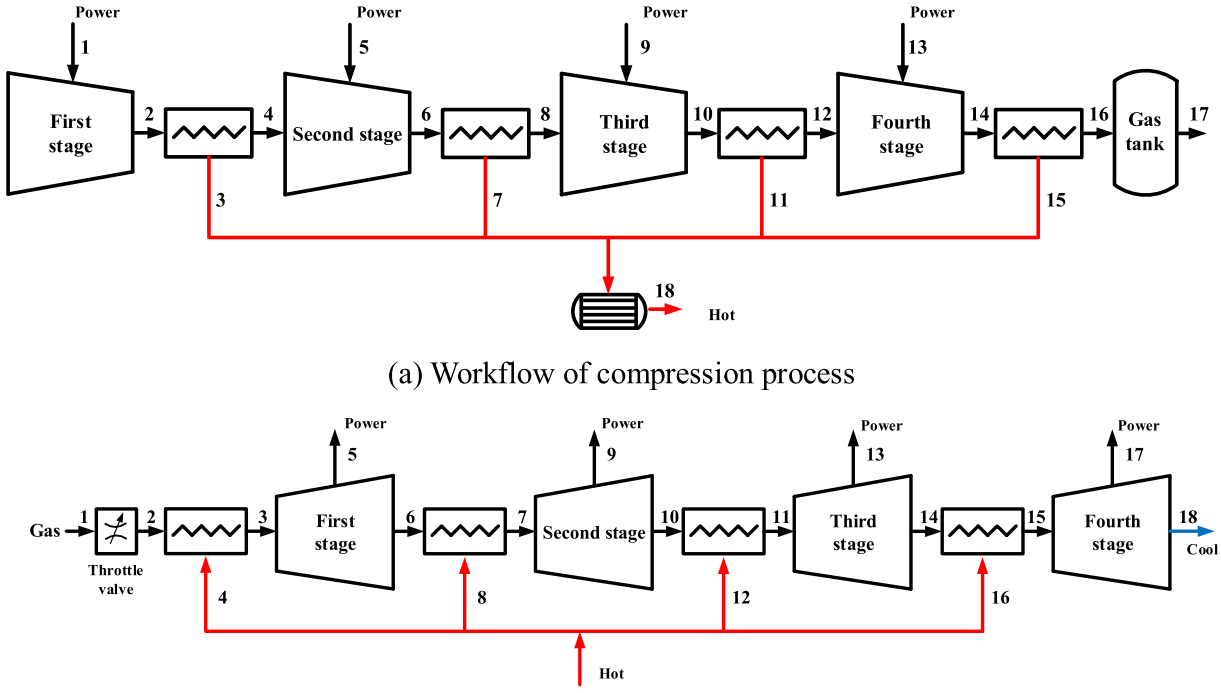

Fig. A.1. The workflow chart multi-stage compressed air energy storage system

The compression process consists of 10 subsystems and 18 streams. According to the coupling relationship between the system and the flow, the thermoeconomic event matrix A_c of the compression process is

$$A_c = \begin{bmatrix} 1 & -1 & 0 & 0 & 0 & 0 & 0 & 0 & 0 & 0 & 0 & 0 & 0 & 0 & 0 & 0 & 0 & 0 \\ 0 & 1 & -1 & -1 & 0 & 0 & 0 & 0 & 0 & 0 & 0 & 0 & 0 & 0 & 0 & 0 & 0 & 0 \\ 0 & 0 & 1 & 1 & -1 & 0 & 0 & 0 & 0 & 0 & 0 & 0 & 0 & 0 & 0 & 0 & 0 & 0 \\ 0 & 0 & 0 & 0 & 0 & 1 & -1 & -1 & 0 & 0 & 0 & 0 & 1 & 0 & 0 & 0 & 0 & 0 \\ 0 & 0 & 0 & 0 & 0 & 0 & 0 & 1 & 1 & -1 & 0 & 0 & 0 & 0 & 0 & 0 & 0 & 0 \\ 0 & 0 & 0 & 0 & 0 & 0 & 0 & 0 & 0 & 1 & -1 & -1 & 0 & 0 & 0 & 0 & 0 & 0 \\ 0 & 0 & 0 & 0 & 0 & 0 & 0 & 0 & 0 & 0 & 0 & 1 & 1 & -1 & 0 & 0 & 0 & 0 \\ 0 & 0 & 0 & 0 & 0 & 0 & 0 & 0 & 0 & 0 & 0 & 0 & 0 & 1 & -1 & -1 & 0 & 0 \\ 0 & 0 & 0 & 0 & 0 & 0 & 0 & 0 & 0 & 0 & 0 & 0 & 0 & 0 & 0 & 1 & -1 & 0 \\ 0 & 0 & 0 & 0 & 0 & 0 & 0 & 0 & 0 & 0 & 0 & 0 & 0 & 0 & 0 & 0 & 0 & -1 \end{bmatrix} \tag{A.1}$$

The energy cost matrix of the compression process is

$$F_c = [F_{c1}\ F_{c2}\ F_{c3}\ F_{c4}\ F_{c5}\ F_{c6}\ F_{c7}\ F_{c8}\ F_{c9}\ F_{c10}\ F_{c11}\ F_{c12}\ F_{c13}\ F_{c14}\ F_{c15}\ F_{c16}\ F_{c17}\ F_{c18}]^T \tag{A.2}$$

In (A.2), $F_{ci} = f_{ci} \times e_{ci}$, f_{ci} is the unit energy cost of the i-th stream, e_{ci} is the exergy of the i-th stream.

The non-energy cost vector Z_c of each subsystem is

$$Z_c = [Z_{c1} \;\; Z_{c2} \;\; Z_{c3} \;\; Z_{c4} \;\; Z_{c5} \;\; Z_{c6} \;\; Z_{c7} \;\; Z_{c8} \;\; Z_{c9} \;\; Z_{c10}]^T \tag{A.3}$$

Available from the thermoeconomic cost equation

$$A_c \times F_c + Z_c = 0 \tag{A.4}$$

In order to solve the matrix equation (A.4), several supplementary matrix equation are established to ensure full rank. Wherein the exergy cost of the input power flow 1, 5, 9, 13 is the known amount. In addition, considering the energy flow released by the interstage cooling process in the compression subsystem as part of the compressed air energy flow, there are

$$\frac{F_{c3}}{e_{c3}} = \frac{F_{c4}}{e_{c4}} \tag{A.5}$$

$$\frac{F_{c7}}{e_{c7}} = \frac{F_{c8}}{e_{c8}} \tag{A.6}$$

$$\frac{F_{c11}}{e_{c11}} = \frac{F_{c12}}{e_{c12}} \tag{A.7}$$

$$\frac{F_{c15}}{e_{c15}} = \frac{F_{c16}}{e_{c16}} \tag{A.8}$$

So, the supplemental relationship matrix is

$$A_c^{'} = \begin{bmatrix} 1 & 0 & 0 & 0 & 0 & 0 & 0 & 0 & 0 & 0 & 0 & 0 & 0 & 0 & 0 & 0 & 0 & 0 \\ 0 & 0 & 0 & 0 & 1 & 0 & 0 & 0 & 0 & 0 & 0 & 0 & 0 & 0 & 0 & 0 & 0 & 0 \\ 0 & 0 & 0 & 0 & 0 & 0 & 0 & 0 & 1 & 0 & 0 & 0 & 0 & 0 & 0 & 0 & 0 & 0 \\ 0 & 0 & 0 & 0 & 0 & 0 & 0 & 0 & 0 & 0 & 0 & 0 & 1 & 0 & 0 & 0 & 0 & 0 \\ 0 & 0 & \frac{1}{e_3} & -\frac{1}{e_4} & 0 & 0 & 0 & 0 & 0 & 0 & 0 & 0 & 0 & 0 & 0 & 0 & 0 & 0 \\ 0 & 0 & 0 & 0 & 0 & 0 & \frac{1}{e_7} & -\frac{1}{e_8} & 0 & 0 & 0 & 0 & 0 & 0 & 0 & 0 & 0 & 0 \\ 0 & 0 & 0 & 0 & 0 & 0 & 0 & 0 & 0 & 0 & \frac{1}{e_{11}} & -\frac{1}{e_{12}} & 0 & 0 & 0 & 0 & 0 & 0 \\ 0 & 0 & 0 & 0 & 0 & 0 & 0 & 0 & 0 & 0 & 0 & 0 & 0 & 0 & \frac{1}{e_{15}} & -\frac{1}{e_{16}} & 0 & 0 \end{bmatrix} \tag{A.9}$$

The supplemental non-energy cost matrix is

$$Z_c^{'} = \left[-c_{grid} \;\; -c_{grid} \;\; -c_{grid} \;\; -c_{grid} \;\; 0 \;\; 0 \;\; 0 \;\; 0\right]^T \tag{A.10}$$

The expansion process consists of 9 subsystems and 18 streams. Similarly, the thermoeconomic event matrix A_e of the expansion process is

$$A_e = \begin{bmatrix} 1 & -1 & 0 & 0 & 0 & 0 & 0 & 0 & 0 & 0 & 0 & 0 & 0 & 0 & 0 & 0 & 0 & 0 \\ 0 & 1 & -1 & 1 & 0 & 0 & 0 & 0 & 0 & 0 & 0 & 0 & 0 & 0 & 0 & 0 & 0 & 0 \\ 0 & 0 & 1 & 0 & -1 & -1 & 0 & 0 & 0 & 0 & 0 & 0 & 0 & 0 & 0 & 0 & 0 & 0 \\ 0 & 0 & 0 & 0 & 0 & 1 & -1 & 1 & 0 & 0 & 0 & 0 & 0 & 0 & 0 & 0 & 0 & 0 \\ 0 & 0 & 0 & 0 & 0 & 0 & 1 & 0 & -1 & -1 & 0 & 0 & 0 & 0 & 0 & 0 & 0 & 0 \\ 0 & 0 & 0 & 0 & 0 & 0 & 0 & 0 & 0 & 1 & 0 & -1 & 1 & 0 & 0 & 0 & 0 & 0 \\ 0 & 0 & 0 & 0 & 0 & 0 & 0 & 0 & 0 & 0 & 1 & 0 & -1 & -1 & 0 & 0 & 0 & 0 \\ 0 & 0 & 0 & 0 & 0 & 0 & 0 & 0 & 0 & 0 & 0 & 0 & 0 & 1 & -1 & -1 & 0 & 0 \\ 0 & 0 & 0 & 0 & 0 & 0 & 0 & 0 & 0 & 0 & 0 & 0 & 0 & 0 & 1 & 0 & -1 & -1 \end{bmatrix} \tag{A.11}$$

The energy cost matrix of the expansion process is

$$F_e = [F_{e1}\ \ F_{e2}\ \ F_{e3}\ \ F_{e4}\ \ F_{e5}\ \ F_{e6}\ \ F_{e7}\ \ F_{e8}\ \ F_{e9}\ \ F_{e10}\ \ F_{e11}\ \ F_{e12}\ \ F_{e13}\ \ F_{e14}\ \ F_{e15}\ \ F_{e16}\ \ F_{e17}\ \ F_{e18}]^T \tag{A.12}$$

In (A.12), $F_{ej} = f_{ej} \times e_{ej}$, f_{ej} is the unit energy cost of the j-th stream, e_{ej} is the exergy of the j-th stream.

The non-energy cost vector Z_e of each subsystem is

$$Z_e = [Z_{e1}\ \ Z_{e2}\ \ Z_{e3}\ \ Z_{e4}\ \ Z_{e5}\ \ Z_{e6}\ \ Z_{e7}\ \ Z_{e8}\ \ Z_{e9}\ \ Z_{e10}]^T \tag{A.13}$$

Thermoeconomic expression of the expansion process is

$$A_e \times F_e + Z_e = 0 \tag{A.14}$$

Similarly, the supplementary equations are established to solve (A.14). Wherein the exergy cost of the input flow 1, 4, 8, 12, 16 is the known amount, which are the price of gas storage and price of hot storage calculated by compression process. In addition, considering the power released by the turbine as part of the compressed air energy flow, there are

$$\frac{F_{e5}}{e_{e5}} = \frac{F_{e6}}{e_{e6}} \tag{A.15}$$

$$\frac{F_{e9}}{e_{e9}} = \frac{F_{e10}}{e_{e10}} \tag{A.16}$$

$$\frac{F_{e13}}{e_{e13}} = \frac{F_{e14}}{e_{e14}} \tag{A.17}$$

$$\frac{F_{e17}}{e_{e17}} = \frac{F_{e18}}{e_{e18}} \tag{A.18}$$

So, the supplemental relationship matrix of expansion process is

$$A_e^{'} = \begin{bmatrix}
1 & 0 & 0 & 0 & 0 & 0 & 0 & 0 & 0 & 0 & 0 & 0 & 0 & 0 & 0 & 0 & 0 & 0 \\
0 & 0 & 0 & 1 & 0 & 0 & 0 & 0 & 0 & 0 & 0 & 0 & 0 & 0 & 0 & 0 & 0 & 0 \\
0 & 0 & 0 & 0 & 0 & 0 & 0 & 1 & 0 & 0 & 0 & 0 & 0 & 0 & 0 & 0 & 0 & 0 \\
0 & 0 & 0 & 0 & 0 & 0 & 0 & 0 & 0 & 0 & 0 & 1 & 0 & 0 & 0 & 0 & 0 & 0 \\
0 & 0 & 0 & 0 & 0 & 0 & 0 & 0 & 0 & 0 & 0 & 0 & 0 & 0 & 0 & 1 & 0 & 0 \\
0 & 0 & 0 & 0 & \frac{1}{e_5} & -\frac{1}{e_6} & 0 & 0 & 0 & 0 & 0 & 0 & 0 & 0 & 0 & 0 & 0 & 0 \\
0 & 0 & 0 & 0 & 0 & 0 & 0 & 0 & \frac{1}{e_9} & -\frac{1}{e_{10}} & 0 & 0 & 0 & 0 & 0 & 0 & 0 & 0 \\
0 & 0 & 0 & 0 & 0 & 0 & 0 & 0 & 0 & 0 & 0 & 0 & \frac{1}{e_{13}} & -\frac{1}{e_{14}} & 0 & 0 & 0 & 0 \\
0 & 0 & 0 & 0 & 0 & 0 & 0 & 0 & 0 & 0 & 0 & 0 & 0 & 0 & 0 & 0 & \frac{1}{e_{17}} & -\frac{1}{e_{18}}
\end{bmatrix} \tag{A.19}$$

The supplemental non-energy cost matrix is

$$Z_e^{'} = \left[-c_{gas} \quad -c_{TES} \quad -c_{TES} \quad -c_{TES} \quad -c_{TES} \quad 0 \quad 0 \quad 0 \quad 0\right]^T \qquad (A.20)$$

References

[1] Mathiesen BV, Lund H, Connolly D, et al. Smart Energy Systems for coherent 100% renewable energy and transport solutions[J]. Appl Energy 2015;145:139–54.

[2] Chen Haisheng, Thang N, Yang Wei. etc. Progress in electrical energy storage system: a critical review [J]. Prog Nat Sci 2009;19(3):291–312.

[3] Lund Henrik, Werner Sven, Wiltshire Robin. 4th Generation District Heating (4GDH): integrating smart thermal grids into future sustainable energy systems. J Energy 2014;68:1–11.

[4] Elbasuony GS, Aleem SHEA, Ibrahim AM, et al. A unified index for power quality evaluation in distributed generation systems[J]. Energy 2018;149:607–22.

[5] Chu S, Majumdar A. Opportunities and challenges for a sustainable energy future[J]. Nature 2012;488:294–303.

[6] Jiang Y, Xu J, Sun Y, Wei C, Wang J, Liao S, Ke D, Li X, Yang J, Peng X. Coordinated operation of gas-electricity integrated distribution system with multi-CCHP and distributed renewable energy sources[J]. Appl Energy 2018;211:237–48.

[7] Gao P, Dai Y, Tong YW, et al. Energy matching and optimization analysis of waste to energy CCHP(combined cooling, heating and power) system with exergy and energy level[J]. Energy 2014;79:522–35.

[8] Wu Z, Gu W, et al. Modeling, planning and optimal energy management of combined cooling, heating and power microgrid: a review[J]. Int J Electr Power Energy Syst 2014;54:26–37.

[9] Dunn B, Kamath H, Tarascon JM. Electrical energy storage for the grid: a battery of choices [J]. Science 2011;334(6058):928–35.

[10] Ferreira HL, Garde R, Fulli G, et al. Characterisation of electrical energy storage technologies[J]. Energy 2013;53:288–98.

[11] Sciacovelli A, Li Y, Chen H, et al. Dynamic simulation of Adiabatic Compressed Air Energy Storage (A-CAES) plant with integrated thermal storage – link between components performance and plant performance[J]. Appl Energy 2017;185(part_P1):16–28.

[12] Facci A, Sanchez D, et al. Trigenerative micro compressed air energy storage: concept and thermodynamic assessment[J]. Appl Energy 2015;158:243–54.

[13] Safaei H, Keith DW, Hugo RJ. Compressed air energy storage (CAES) with compressors distributed at heat loads to enable waste heat utilization [J]. Appl Energy 2013;103:165–79.

[14] Li Y, Wang X, Li D, et al. A trigeneration system based on compressed air and thermal energy storage [J]. Appl Energy 2012;99:316–23.

[15] Adriano, Sciacovelli, Yongliang, et al. Dynamic simulation of Adiabatic Compressed Air Energy Storage (A-CAES) plant with integrated thermal storage – link between components performance and plant performance [J]. Appl Energy 2017;185:16–28.

[16] Venkataramani G, Vijayamithran P, Ding YL, et al. Thermodynamic analysis on compressed air energy storage augmenting power/polygeneration for roundtrip efficiency enhancement [J]. Energy 2019;180:107–20.

[17] Lv S, He W, et al. Modelling and analysis of a novel compressed air energy storage system for trigeneration based on electrical energy peak load shifting [J]. Energy Convers Manag 2017;135:394–401.

[18] Jiang RH, Qin FGF, Chen BM, Yang XP, Yin HB, et al. Thermodynamic performance analysis, assessment and comparison of an advanced trigenerative compressed air energy storage system under different operation strategies [J]. Energy 2019:186.

[19] Jiang RH, Yin H, Yang M, et al. Thermodynamic model development and performance analysis of a novel combined cooling, heating and power system integrated with trigenerative compressed air energy storage[J]. Energy Convers Manag 2018;168:49–59.

[20] Han ZH, Guo SC. Investigation of operation strategy of combined cooling, heating and power(CCHP) system based on advanced adiabatic compressed air energy storage [J]. Energy 2018;160:290–308.

[21] Wu D, Han ZH, Liu Z, Zhang H. Study on configuration optimization and economic feasibility analysis for combined cooling, heating and power system, vol. 190. Energy Conversion and Management; 2019. p. 91–104.

[22] Feng Lj, Dai Xy, el al. Analysis of energy-matching performance and suitable users of conventional CCHP systems coupled with different energy storage systems [J]. Energy Conversion and Management; 2019. p. 200.

[23] Wang HR, Yao, et al. Thermo-economic optimization of a combined cooling, heating and power system based on small-scale compressed air energy storage [J]. Energy Convers Manag 2016;118:377–86.

[24] Marechal, Francois, Wang, et al. Multi-objective optimization and exergoeconomic analysis of a combined cooling, heating and power based compressed air energy storage system [J]. Energy Convers Manag 2017;168:199–209.

[25] Jabari F, Nojavan S, et al. Designing and optimizing a novel advanced adiabatic compressed air energy storage and air source heat pump based m-Combined Cooling, heating and power system [J]. Energy 2016;116:64–77.

[26] Yan Y, Zhang C, Li K, et al. An integrated design for hybrid combined cooling, heating and power system with compressed air energy storage[J]. Appl Energy 2017;210:1151–66.

[27] Wang X, Yang C, Huang M, et al. Off-design performances of gas turbine-based CCHP combined with solar and compressed air energy storage with organic Rankine cycle[J]. Energy Convers Manag 2018;156:626–38.

[28] Yang K, Zhang Y, Li X, et al. Theoretical evaluation on the impact of heat exchanger in advanced adiabatic compressed air energy storage system[J]. Energy Convers Manag 2014;86:1031–44.

[29] Evins R, Orehounig K, Dorer V, et al. New formulations of the 'energy hub' model to address operational constraints[J]. Energy 2014;73:387–98.

[30] Da Silva JAM, Santos, Joaquim José, Carvalho M, et al. On the thermoeconomic and LCA methods for waste and fuel allocation in multiproduct systems[J]. Energy 2017;127:775–85.

[31] Erlach B, Serra L, Valero A. Structural theory as standard for thermoeconomics [J]. Energy Convers Manag 1999;40(15–16):1627–49.

[32] Lozano MA, Valero A. Theory of the exergetic cost[J]. Energy 1993;18(9):939–60.

[33] Zhao P, Gao L, Wang J, et al. Energy efficiency analysis and off-design analysis of two different discharge modes for compressed air energy storage system using axial turbines[J]. Renew Energy 2016;85:1164–77.

[34] Farrar M. Striped Smith–Waterman speeds database searches six time over other SIMD implementations[J]. Bioinformatics 2007;23(2):156–61.